RSC Sustainability

ROYAL SOCIETY OF CHEMISTRY

PAPER

View Article Online
View Journal | View Issue

Cite this: *RSC Sustainability*, 2026, **4**, 962

Polymer/iron-oxide nanocomposite adsorbents for cycled magnetically-enabled extraction of aqueous micropollutants

Eoin P. M^cKiernan, [a] Alexa Ennis, [b] Colm Delaney, [b] Larisa Florea [b] and Dermot F. Brougham *[a]

We present a facile, low-cost method for the preparation of milli-scale magnetic polymer prints which can be utilized as adsorbents for removal of methylene blue (MB) from aqueous solution. The nanocomposites were prepared by mixing magnetic iron-oxide nanoflowers (NFs) with a multi-branched acrylate terminated PEG monomer (Trimethylolpropane ethoxylate Triacrylate, TET). 1 mol% phenylbis (2,4,6-trimethylbenzoyl) phosphine oxide (BAPO) was used as a photoinitiator, enabling very rapid bulk template printing by UV-initiated free radical polymerization. The magnetic adsorbents demonstrated moderate adsorption capacity of 0.75 mg g^{-1}, however a 5 wt% adsorbent load could remove over 99% of dissolved MB at concentrations as high as 15 mg L^{-1}. The materials were homogeneous and were easily processable into a range of shapes. Full characterization of the magnetic adsorbents was undertaken, including determination of the dependence of adsorption capacity on adsorbent volume and surface area to volume ratio. A morphology (cylinders of $d = 3$ mm, $h = 1$ mm) was identified that provided optimal adsorption performance and which enabled rapid magnetic capture/recovery for subsequent regeneration by solvent extraction. Facile capture, as compared with nano- or micro-scale absorbents, offers practical advantages for in-line continuous extraction. The magnetic adsorbent showed excellent stability and could be regenerated at least 5 times without any observed decrease in adsorption efficiency. Evaluation of the performance of the adsorbent with a library of common micropollutants revealed the dominant role of, polymer to MB, n–π interactions in the micropollutant extraction mechanism.

Received 23rd August 2025
Accepted 18th December 2025

DOI: 10.1039/d5su00701a

rsc.li/rscsus

Sustainability spotlight

Our work advances sustainable chemistry by describing the first milli-scale magnetic adsorbent for extraction of a range of micropollutants from aqueous flows. The literature focuses on nanoscale adsorbents, which are difficult to recover. We used macromer compatible nanoparticle surface chemistry to maintain particle dispersion, facilitating polymerization into a range of adsorbent sizes/shapes for multiple applications. We optimized adsorbent size, shape and particle loading for methylene blue extraction, while retaining facile recovery. We demonstrated regeneration of the adsorbents without damage, using relatively benign ethanol extraction. The study is aligned squarely with UN Sustainable Development Goal 6 'Clean Water and Sanitation', and also with Goal 9 'Industry Innovation and Infrastructure' and also Goals 14 'Life below Water'' and 15 'Life on Land'.

Introduction

More than one third of the earth's available freshwater is used in industrial, agricultural and domestic processes which leave it contaminated with various species including dyes, pesticides, and heavy metals.[1] Many industrial wastewater systems, particularly those produced by the textile industry, contain significant quantities of cationic dyes, which can be difficult to purge from high volume systems due to their high aqueous solubility and low biodegradability.[2] This has led to significant contamination of surface and ground water.[3] The removal of cationic dyes from industrial wastewater has been an area of significant research interest due to their negative environmental[4] and human health effects.[5] Methylene blue (MB) which is used in the leather and silk industries, is a non-biodegradable, carcinogenic heterocyclic aromatic dye. At high concentrations MB has been associated with health impacts including blindness, and respiratory and mental disorders.[6] Due to its high molar adsorption coefficient (~8.4 × 10^4 L mol^{-1} cm^{-1} at 644 nm) even low concentrations of MB can have devastating effects on aquatic environments. By reducing

[a]School of Chemistry, University College Dublin, Belfield, Dublin 4, Ireland. E-mail: dermot.brougham@ucd.ie
[b]School of Chemistry & AMBER, The SFI Research Centre for Advanced Materials and BioEngineering Research, Trinity College Dublin, The University of Dublin, Ireland

light transmittance through water MB can reduce photosynthetic activity of aquatic life/lower dissolved oxygen.[7] Its strong absorbance also means it is an ideal micropollutant for developing extraction systems.

A wide range of approaches have been investigated for removal of dyes such as MB from wastewater. Physical approaches include filtration and adsorption, and there are also electrochemical, photocatalytic and microbiological treatments.[8] The advantages of the physical approaches are that they generally do not degrade the dye, which can generate toxic side products,[9] and they are generally more simple and more flexibly implemented.[10] However membranes and adsorbents usually require periodic (and costly) replacement.[11] Hence there is need for self-regenerating systems. This work provides adsorbents that could be used in such systems.

Currently the standard treatment of wastewater with such contaminants is a combination of activated carbon adsorption, chemical oxidation and biological treatments.[12] However, activated carbon has yet to be adopted for widescale industrial use, due to significant costs associated with its production and regeneration.[13,14] For waste water applications physisorption is often the preferred mode, with ion exchange, electrostatic, hydrogen bonding, Van der Waals forces, hydrophobic and π–π interactions all reported.[15] The functional groups present in the matrix largely determine its mode of interaction with the targeted pollutants.[16] Polymer-based adsorbents have advantages including a range of possible functionalities, low initial costs and potential for reusability. Polymers used for wastewater treatment include ion exchange resins,[17–19] polysaccharides,[20,21] organic polymers[22,23] and magnetic-polymer composites.[24,25] For adsorption of cationic dyes synthetic polymers studied typically contain ionizable function groups (*i.e.* hydroxyl, carboxyl) which can facilitate attractive electrostatic and hydrogen bonding interactions.

Organic polymer matrices have been used extensively in wastewater treatment. They generally take the form of porous organic polymers (POPs) or interpenetrating polymer networks (IPNs). POPs are materials consisting of networks of pores connected by covalent bonds. Their large surface areas and tuneable porosities makes them of particular interest for dye adsorption.[26] However they are often limited by low dye removal rates and complicated synthetic processes using high cost monomers.[27] Functionalization of POPs with moieties including azobenzenes[28,29] or triazines[27,30,31] has been reported to improve dye adsorption capacities and removal rates. IPNs contain two or more polymer networks that, while entangled on a molecular level, are not covalently bound to one another.[32] They have attracted interest for dye adsorption due to their stability and high swelling capacity.[33] A polymethacrylic acid grafted cellulose and bentonite IPN was shown to be an effective adsorbent for MB removal from aqueous solutions.[34] Under optimized conditions of pH and temperature it was found that an IPN formed from carboxymethyl chitosan and poly(2-(dimethylamino)ethyl) methacrylate could simultaneously remove the anionic dye indigo carmine and the cationic dye safranin T from aqueous solution.[35]

The recovery of adsorbents after use must also be considered in any water treatment process. The need for centrifugation and/or filtration adds to the cost and complexity of the process as well as limiting throughput. By including a magnetic component, separation of the adsorbent can be easily achieved using the field gradient provided by an external magnet.[36–38] Magnetic composites for dye removal generally fall into two categories; water dispersions of magnetic nano/microparticles with polymer coatings, and bulk polymer matrices with embedded magnetic particles. Magnetic nanoparticle (NP) dispersions are often used as adsorbents due to their high surface area to volume ratio (SA/Vol) and fast re-dispersion on removal of the magnet.[39–41] SDS modified maghemite (γ-Fe_2O_3) NPs have been used as an efficient method of removing cationic dyes from aqueous solutions by magnetic capture.[42] Coating $MnFe_2O_4$ NPs with polyacrylic acid was shown to significantly improve the MB adsorption capacity as compared to the uncoated particles.[43] On the other hand, incorporation of magnetic NPs into bulk polymer matrices enables facile retrieval of the adsorbent/reduces losses in waste streams that would be difficult to avoid for dispersed NPs. A pH responsive magnetically-capturable bulk hydrogel of acrylic acid and vinyl sulfonic acid with embedded superparamagnetic iron oxide nanoparticles (SPIONs) was shown to have reasonably good adsorption capacity for MB.[44]

The objective of the work was to develop retrievable adsorbents for common industrial micropollutants using macromonomers that also provide processability for downstream advanced manufacturing/patterning applications. Realising these goals required optimization of magnetic particle dispersion in the selected formulations, and development of understanding into both the adsorbent size-dependent swelling/adsorption responses and the molecular mechanisms of adsorption. The adsorbent selected was trimethylolpropane ethoxylate triacrylate (TET), which to our knowledge has not been reported for dye removal or wastewater treatment. TET is an inexpensive commercial macromer, available in a range of molecular weights. In the absence of anionic groups, Fig. 1, adsorption is expected to be due to lone pair – π interactions, *i.e.* the association between the electron lone pairs on the oxygen atoms of the ethoxylate side chains and the electron-poor π system of MB.[45] As the molecular weight of TET increases, the number of ethoxylate groups in the side chains grows as does the ratio of the oxygen bearing ethoxylate groups to the non-interacting ethyl and methyl groups of the polymer. So, in principle, higher TET molecular weight should increase the number of available adsorption sites per unit mass of polymer. Hence the impact of the chain length on the adsorption efficiency of the adsorbent was examined by measuring the MB adsorption capacity of TET polymers prepared using the three commercially available molecular weights (428, 612 and 912 g mol^{-1}). TET adsorbents were found to be fully regeneratable for cycled use. Regeneratable and magnetically retrievable TET adsorbents were prepared by dispersing magnetic iron-oxide nanoflowers (NFs) in the polymerization medium before photopolymerization. An optimal physical size and composition of the magnetic adsorbent (NF-TET) that

maximized adsorption and enabled facile magnetic capture/physical recovery was identified. Finally the adsorption mechanism was identified by analysing the materials capacity to remove different micropollutants.

Results and discussion

Magnetic polymer formulation, primary physical characterization, and adsorbent design

Macroscale polymer adsorbents were formed using TET macromonomers of different molecular weight, both with and without the inclusion of multi-core γ-Fe_2O_3 nanoparticles (or nanoflowers, NFs), by facile BAPO-initiated free radical polymerization, as described in Experimental and shown in Scheme 1. The NFs were synthesized using our established procedure,[46] see Experimental, and were used without post-synthesis surface modification. Formation of homogeneous pre-polymerization formulations was facile, even with NFs included, and was ensured by agitation using a benchtop vortexer. In all cases polymerization was complete within 10 minutes, providing robust solid magnetic and non-magnetic adsorbents that could be easily handled, used and re-used, see below. Detailed characterization of the magnetic composites is provided in Fig. S1. A series of polydimethylsiloxane (PDMS) templates were fabricated for production. These provided transparent (and so homogeneous on micro-scale) adsorbent cylinders and disks of highly reproducible mass, shape, and surface area. This processability enabled rapid production of large quantities of essentially identical adsorbents for evaluating the effect of different factors, *e.g.* of adsorbent load, while keeping the

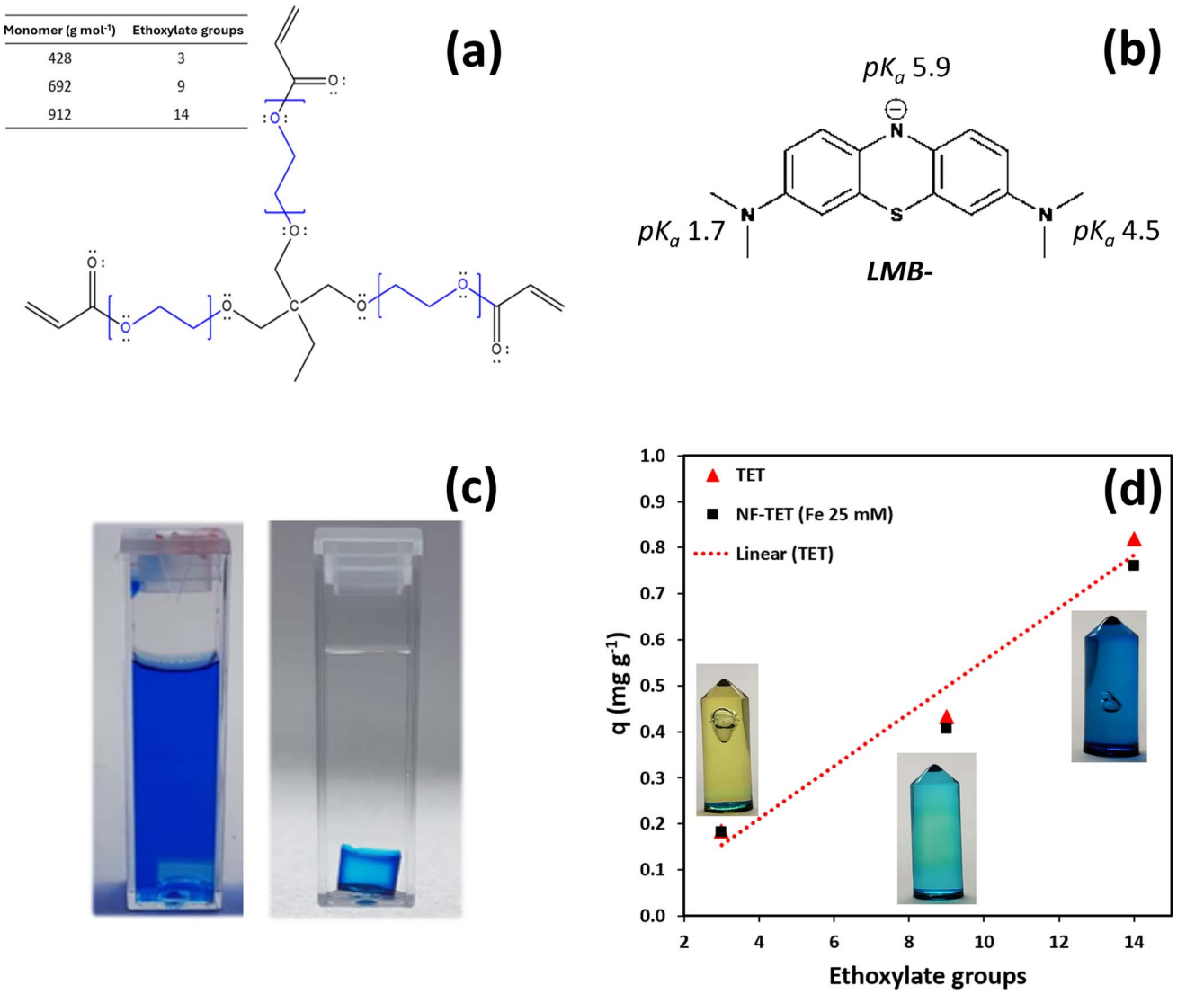

Fig. 1 (a) Chemical structures and molecular weights of the TET macromonomers used, and (b) of methylene blue, shown in the LMB-form. (c) Photographs of a TET912 cuboid (7.2 × 7.2 × 5.2 mm, formed inside a standard disposable cuvette lid) immediately after immersion in a 100 mg L^{-1} MB solution (left) and following adsorption to saturation, demonstrating dye retention in the adsorbent. (d) Dependence of maximum MB adsorption capacity (q) on the number of ethoxylate groups in TET, determined at 1 wt% of adsorbent in 3 mL of 100 mg L^{-1} MB solutions for cylindrical TET (photographs shown) and NF-TET (at 0.2 wt%, ~25 mM Fe) adsorbents.

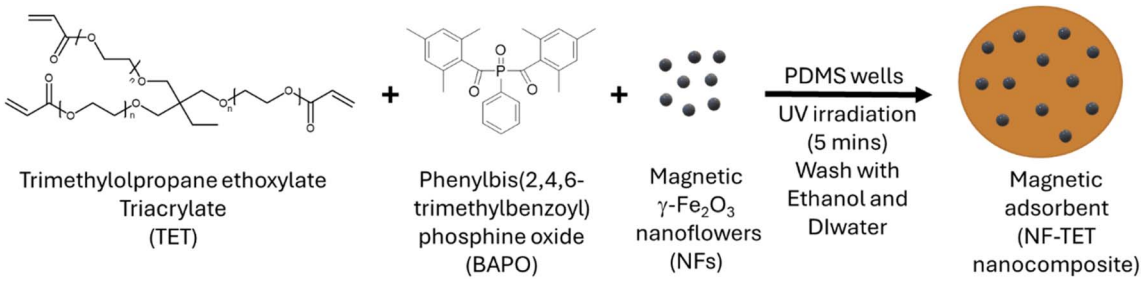

Scheme 1 Visual representation of NF-TET nanocomposite formation.

adsorbent SA/Vol constant. Inclusion of NFs, at 0.2 wt%, equivalent to ~25 mM Fe, did not disrupt the processability or outer appearance for the adsorbents, but enabled rapid isolation/separation of the magnetic adsorbents (NF-TET) using a permanent magnet. We have demonstrated, using DLS, that NFs are fully dispersed in TET under the preparation conditions used, Fig. S2. While that is important for retention of some magnetic properties, *e.g.* the AC-field hyperthermic response, the translational magnetic force generated by an external magnet is primarily determined by the particle loading in the adsorbent.

Large adsorbents, of 4 mL volume, were first prepared using TET monomers of molecular weight 428, 612 and 912 g mol^{-1} (with and without including of NFs). The steady state adsorption capacity, q (reported here in mg g^{-1}), was then determined under identical conditions, Fig. 1d, from the absorbance of the depleted solutions (the values of which were found to be unchanging after 24 h, see Experimental). Carboxymethyl cellulose hydrogels,[47] and other matrices have higher reported MB adsorption however, as discussed below, q is not necessarily the limiting factor and the NF-TET system has other advantages. The q values were found to increase strongly with the number of ethoxylate groups per monomer unit, Fig. 1d. This suggests that MB adsorption occurs predominantly through interactions with the oxygen atoms on the polymer chains, we return to the mechanism below. TET912, the highest commercially available molecular weight, showed the highest q and so was used for the rest of the study. Critically, the inclusion of NFs at 0.2 wt% had marginal, if any, effect on adsorption capacity (as expected given the minimal macromonomer/NF interactions, Fig. s2) while providing rapid magnetic separation. So the magnetic loading was fixed at this value for the rest of the study. On adsorption of MB the TET912 adsorbents (which were initially colourless and transparent) became strongly blue-coloured as expected, Fig. 2a and b. For NF-TET912, due to the presence of γ-Fe_2O_3, the disks are strongly brown coloured, Fig. 3a, and no significant change in colour was apparent on adsorption.

Larger adsorbents have advantages for magnetic capture and are less likely to accumulate on surfaces or block channels within vessels/reactors. However their reduced SA/Vol may reduce the MB adsorption rate, and could also affect the MB adsorption capacity. Cylindrical TET912 adsorbents were

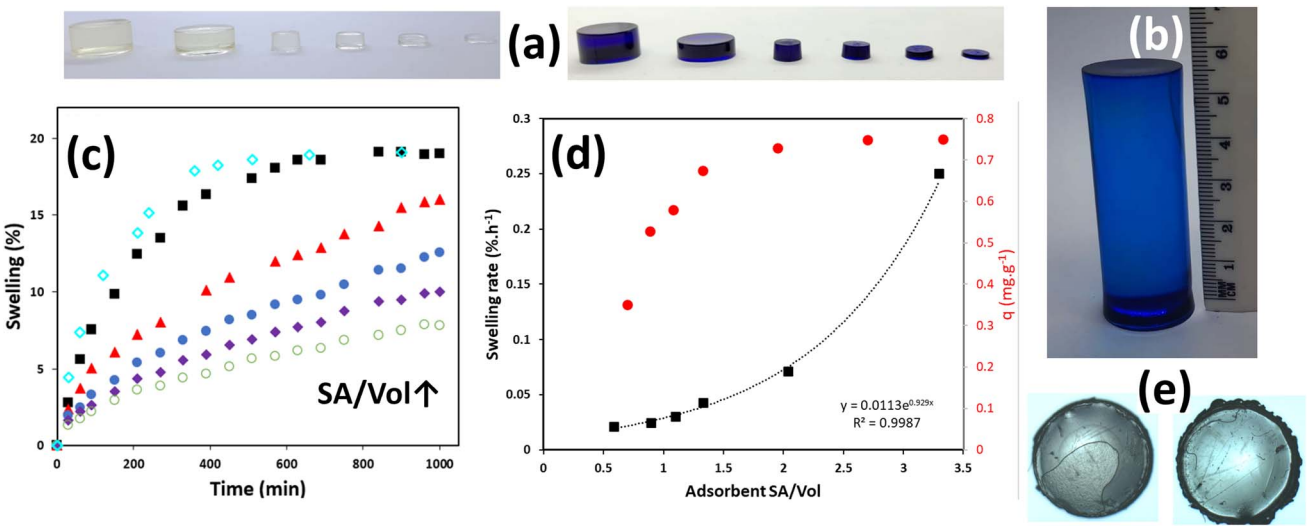

Fig. 2 (a) Photographs; of TET912 adsorbents cast at different total vol with varied SA/Vol (left) and of the equivalent 0.2 wt% NF-TET912 adsorbents (right, following MB adsorption), and (b) of an upscaled TET912 adsorbent following extraction of MB. (c) Swelling at laboratory temperature, after curing and casting, for the six different SA/Vol non-magnetic TET912 adsorbents shown in (2a), determined gravimetrically as swelling progressed in 100 mg L^{-1} MB. (d) Dependence of initial swelling rate (the slope of a linear fit, up to 200 min, for the data in (c) and of MB adsorption capacity (q) on SA/Vol for the six adsorbents shown in (a). (e) Optical microscopy images of a TET912 (left) and 0.2 wt% NF-TET912 disk (right).

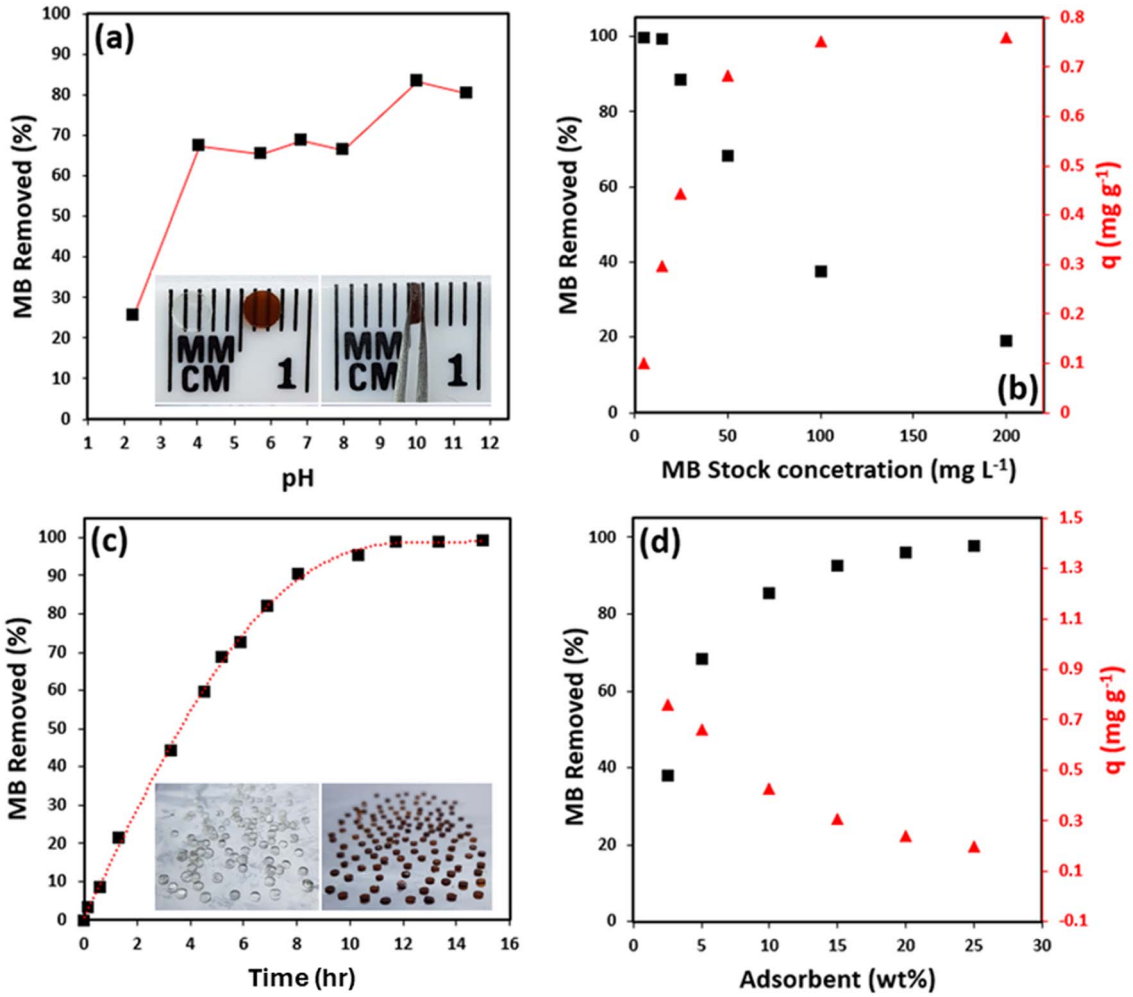

Fig. 3 Effect of adsorption conditions on performance of NF-TET912 disks (0.2 wt% NFs, 7.1 mm^3 vol, SA/Vol 3.3) at LT; (a) pH dependence (5 wt% adsorbent in 50 mg L^{-1} MB solution at pH 7), with (inset) magnetic disks prior to adsorption showing the characteristic brown colour due to the presence of NFs, (b) initial MB concentration (5 wt% adsorbent in 5 mL MB solution at pH7), (c) adsorbent contact time (5 wt% adsorbent in 15 mg L^{-1} MB solution at pH7), (d) adsorbent load (in 5 mL 50 mg L^{-1} MB solution at pH7). Inset are photographic images of an NF-TET912 disk in close-up, and of samples of unloaded and NF-loaded disks.

prepared with varied SA/Vol, all of which appeared homogeneous and transparent (when not NF loaded). The swelling rates, equilibrium swelling and equilibrium q values were measured, Fig. 2, to evaluate the impact of adsorbent size on performance.

The swelling rate was found to be strongly dependent on SA/Vol, as expected. The initial rate showed an exponential increase with SA/Vol, Fig. 2c. The final equilibrium swelling was found to be independent of SA/Vol, with average value (achieved within 24 h in all cases) for the six structures studied of 21.3 ± 0.9% (by mass), Fig. 2c. Hence adsorbents of all sizes studied fully swell but the higher SA/Vol, ones do so far more quickly. On the other hand the equilibrium MB adsorption capacity, q values, increased sharply as the SA/Vol was increased from 0.9 to 1.3, and reached a plateau at 0.75 ± 0.01 $mg.g^{-1}$ for the smallest sized/highest SA/Vol adsorbents, Fig. 2d. So, while water fully penetrates TET912, for lower SA/Vol adsorbents MB molecules occupying adsorption sites towards the outer surface of the adsorbent partially block transport of MB. The fact that the higher SA/Vol adsorbents attain the same q-value demonstrates that they are uniformly loaded/homogeneous. Nevertheless larger, lower SA/Vol, TET cylinders were produced to make a preliminary evaluation of scalability, and as shown in Fig. 2b, the larger structures are efficient adsorbents. For the remainder of this study, to maximize adsorption capacity and adsorption rate and to provide magnetic capture, cylindrical NF-TET912 prints ($d \times h$ of 3 × 1 mm; SA 23.6 mm^2; volume 7.1 mm^3; SA/Vol 3.3 which is on the q-plateau, with 0.2 wt% Fe) were fabricated. These optimized structures, the smallest shown in Fig. 2a, were used in all the following adsorption experiments and will be referred to as "NF-TET912 disks". Optical microscopy shows that inclusion of NFs has no impact on the large scale structure or surface appearance of the disks, Fig. 2e.

TET912 disk adsorbent performance

MB has complex ionization, with pK_a values at pH ~1.7, ~4.5 and ~5.9, Fig. 1b. Hence, while the species present may differ within the pore structure of the adsorbent, it is likely that the

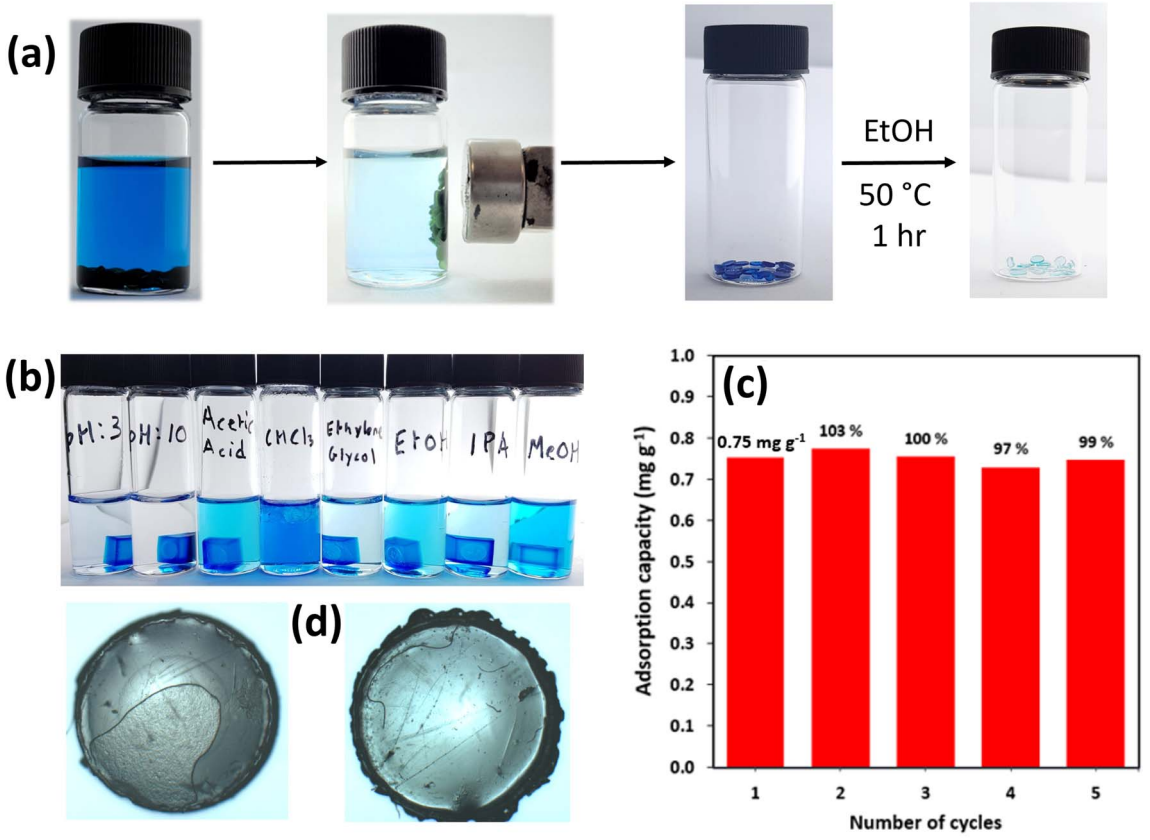

Fig. 4 Photographs of the (a) MB adsorption/magnetic recovery/solvent extraction/disk regeneration process using 7.1 mm^3 NF-TET912 disks, and (b) of extraction solvent selection. (c) Cycled use of the same NF-TET disks demonstrating retention of adsorption capacity (5 wt% adsorbent in 100 mg L^{-1} MB solution) over multiple EtOH extraction/regeneration steps. (d) Optical images of TET912 adsorbents before (left) and after (right) 5 extraction cycles.

adsorption capacity will be impacted by changes in pH altering the surface charging of the analyte at least. The impact of pH on the adsorption capacity of NF-TET912 disks was measured by varying the pH of the MB stock solution at constant adsorbent load (1 wt%) and MB concentration (50 mg L^{-1}). This MB concentration was selected as it is in the upper part of the range associated with industrial wastewater streams, and it has been commonly used in remediation studies.[47] Samples were monitored until the adsorption (from the initial 50 mg L^{-1} solution) had stabilized and q was then measured. MB uptake was most efficient for pH > 8, and a sharp decline in efficiency was observed for pH < 4, Fig. 3a, which interestingly is below the pK_a of the first amine of MB. The capacity is usefully flat in the environmentally relevant pH range of 4–8. All adsorption experiments that follow were performed at pH 7, within the typical range of textile effluents.

The impact of initial MB concentration in the batch solution on the extraction efficiency of NF-TET912 disks was measured to determine the most effective concentration range. Adsorbent load was kept constant at 5 wt% dry (50 g L^{-1}), which is a realizable load for larger volume in-line extractions. It was found that >99% of MB was removed at concentrations up to 15 mg L^{-1}, Fig. 3b. As the MB concentration was further increased, the fraction of dye removed decreased. Above 100 mg mL^{-1} a plateau in capacity, at the SA/Vol plateau value already determined of 0.75 mg g^{-1}, suggests that all adsorption sites are occupied. The adsorption kinetics were then measured in 15 mg L^{-1} MB stock (*i.e.* on the low concentration plateau, Fig. 3b) under gentle agitation on a shaker. It was found that >95% of MB was removed after 10 h and >99% after 15 h, Fig. 3c. The impact of adsorbent load at high MB concentration (50 mg L^{-1}) was also examined. As shown in Fig. 3d increased adsorbent loading resulted in higher removal efficiency. However, at this concentration a loading of 20 wt% was required to remove >90% MB, which may not be practical for larger scale extraction. It can be concluded that NF-TET912 disks are most applicable to waste systems containing ≤25 mg L^{-1} MB, which is in the relevant range.

Adsorbent cyclability is critical for environmental applications. If the adsorbent and extraction solvent can be regenerated, given the advantage of NF-TET912 for rapid adsorption and magnetic capture, possibilities for in-line self-regenerating continuous extraction systems may emerge, which would mitigate the moderate capacity. A schematic representation of a single sequential adsorbent cycle is shown in Fig. 4. An extensive survey identified ethanol as the solvent that provided highest recovery of MB under benign conditions of 50 °C for 1 h, see Experimental. It is also relatively low cost and comparatively

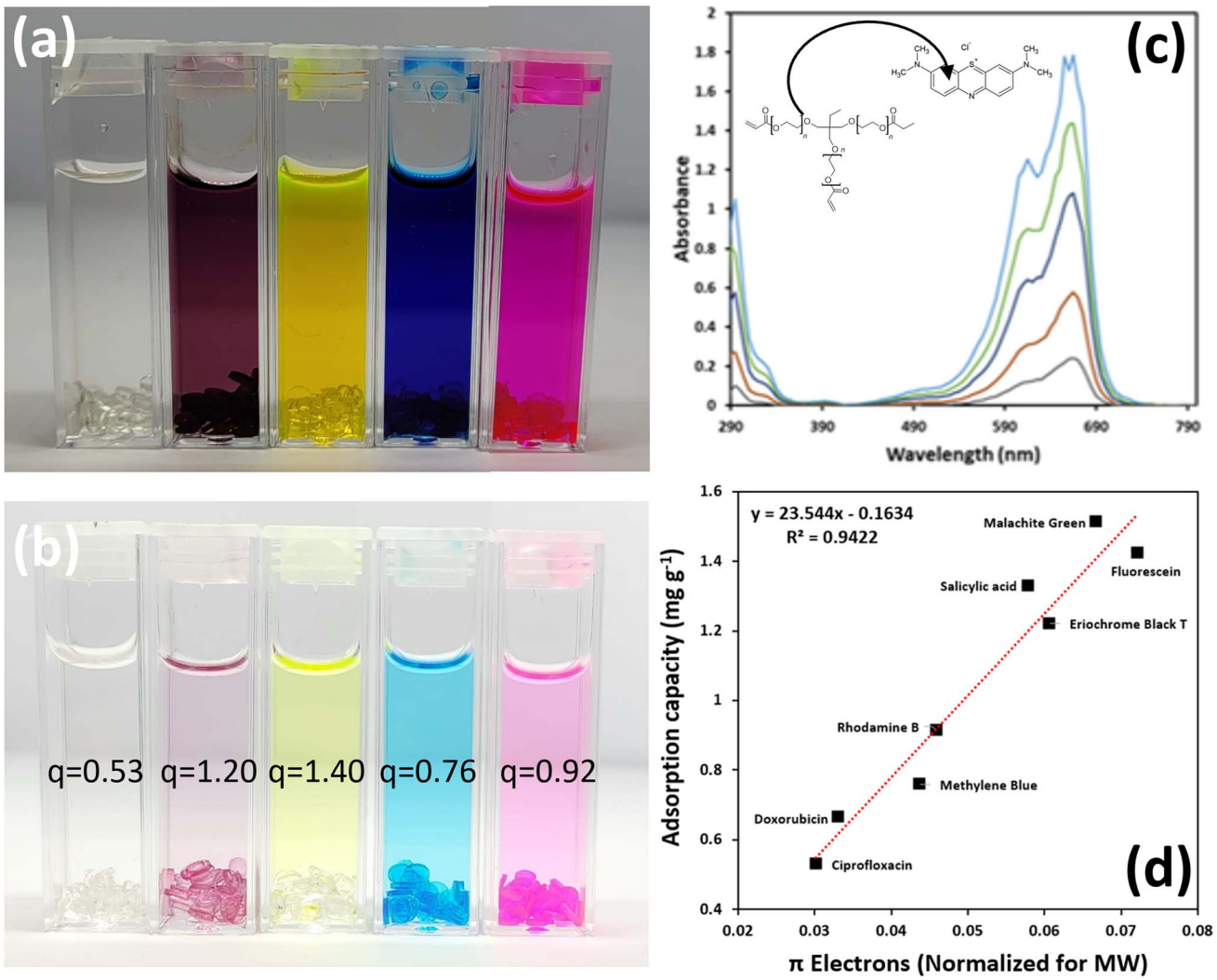

Fig. 5 Photographs of the extraction of dyes/micropollutants using 7.1 mm^3 TET912 disks (unloaded in this case to aid imaging) (a) initially, and (b) at equilibrium. From the left; ciprofloxacin, eriochrome black T, fluorescein, methylene blue, rhodamine B. (c) Exemplar UV-vis spectra (linear standard curves for all micropollutants are provided in SI), inset schematic representation of the suggested n–π interactions. (d) Adsorption capacity of NF-TET912 disks for different micropollutants plotted as a function of the number of π electrons normalized for molecular weight.

low in toxicity. Following EtOH extraction the desorbed MB solution was evaporated and quantified, spectroscopic analysis indicated no change in the dye molecular structure. The adsorbents were then isolated, dried and their adsorption capacity in 100 mg L^{-1} MB solution was re-measured. Reusability/regeneration of NF-TET912 over consecutive adsorption–desorption steps was evaluated and it was found that the disks retained >99% of their MB adsorption capacity after 5 cycles. Furthermore the adsorbents showed no visible signs of degradation, Fig. 4.

Utility of NF-TET912 disks and mechanism of adsorption

Finally we evaluated the utility of NF-TET912 disks for adsorbing water soluble, UV-detectable molecules that have been investigated and published as potential micropollutants in the literature since 2011, or detected in effluents from sewage-treatment plants.[48] The goals were to establish the general utility of NF-TET912 disks and to probe the adsorption mechanism/matrix interactions. Aliev, Pavlakos *et al.* demonstrated that the strength of n – π interactions can be significantly impacted by heteroatom substitution, the presence of electron donating or withdrawing groups, and the molecular geometry of the molecule.[49] So it was expected that the different molecular properties of the analytes, summarized in Table S1-1, would generate significant variation in q.

The adsorption process is illustrated using varying stock concentrations with non-magnetic TET912 disks, for visual clarity, in Fig. 5. NF-TET912 disks were used for the actual quantification and exemplar UV-vis data is shown in Fig. 5, full details are provided in Fig. S3. It was found that the adsorption capacity for this selection of micropollutants varied significantly from 0.53–1.51 mg g^{-1}. The adsorption capacity was cross-plotted against all the available physical parameters, including molecular weight, aqueous solubility, and the

number of H-bond donors and H-bond acceptors. In most cases there was no apparent correlation, Fig. S4. This suggests that these factors play only a minor role in the micropollutant/TET912 adsorption interactions. However a clear positive correlation (R^2 0.94) was found between q and the number of π electrons of each micropollutant normalized for its molecular weight, Fig. 5. This trend strongly suggests that adsorption is driven by the prevalence of n–π interactions across this series, while molecular weight mitigates against the interaction. The reason for the latter is not clear. However this is not a diffusion limitation as in all cases the steady state bulk concentration was achieved/the adsorption had plateaud. The correlation is remarkable given the diverse molecular structures/properties of the selected micropollutants.

Conclusions

The mechanistic study pinpoints the dominant role of n–π interactions in adsorption using TET, which is an unusual finding. It may also enable prediction of capacity, with reasonable certainty, for other analytes. The insights gained may also be relevant for developing NF-TET as a drug delivery platform for future studies. From a practical perspective, we have presented a facile method for preparation of bulk magnetic polymer prints for use as micropollutant adsorbents. The material shows rapid adsorption and excellent regeneration/reusability, properties that are unaffected by the inclusion of NFs at concentrations and adsorbent size that enable rapid magnetic capture. While TET does not achieve adsorption capacities as high as some previously reported micro- and nano-scale polymer materials, the facile and low-cost nature of the template-assisted free-radical polymerization method may be a more applicable for wastewater systems. The high volumes associated with commercial waste require large quantities of adsorbent for effective contaminant removal which makes dispersed nano or microscale adsorbents less attractive. Milli-scale adsorbents, such as NF-TET912 disks, are inexpensive and have several advantages, compared to the more commonly studied dispersed nanoparticulate magnetic adsorbents.[50–52] As noted above, the disks large size makes them less likely to foul surfaces or block channels or filters. More importantly the magnetic force exerted by a field gradient is proportional to the volume of magnetic material per particle.[53] So, given that each NF-TET912 disk contains $\sim 1 - 2 \times 10^{12}$ NFs, their magnetic capture from relatively larger volumes of wastewater is rapid and, unlike with dispersed nanoparticles, usually quantitative.

Experimental

Reagents. All chemicals and reagents are commercially available and used without further purification.

Instrumentation. An Agilent Cary 60 UV-vis Spectrophotometer was used to measure the concentration of MB in aqueous solution. SEM images of magnetic polymers were acquired using a Zeiss Ultra Plus Scanning Electron Microscope, using an accelerating voltage of 3 kV. Prior to SEM imaging, all samples were coated with 10 nm Au–Pd layer using a Cressington Sputter Coater 208HR. Polymerization of the photosensitive monomer solution was performed using a homemade instrument comprising of a light isolating safety box, with 8 LEDs, which were held in place in a 3D-printed ring, the peak wavelength was λ 365 nm and total irradiation power was 16 mW cm^2.

Magnetic nanoflower (NF) preparation. Synthesis of iron oxide nanoflowers was based on the thermal decomposition of iron chloride precursors in organic media and adapted from Hugounenq *et al.*[54] Briefly, in a typical preparation 0.541 g of iron(III) chloride hexahydrate, 0.199 g of iron(II) chloride tetrahydrate and 0.32 g of sodium hydroxide were dissolved in a 37.1 mL (1 : 1 by volume) mixture of DEG and NMDEA in a 100c mL round bottom flask. The resulting mixture was magnetically stirred for 3 h. Then, the temperature was increased to 220 °C at 5 °C min^{-1} by placing the round bottom flask in temperature-controlled heating mantle. The suspension was heated with magnetic stirring for 12 h, and then allowed to cool to room temperature. The black sediments were separated magnetically and washed with 10 mL portions of a mixture (1 : 1 by volume) of ethanol and ethyl acetate 3 times to remove impurities. Possible iron hydroxides were removed by treatment with 10 mL 10% nitric acid for 15 min 4.125 g sample of iron(III) nitrate nonahydrate was then dissolved in 10 mL of water and added to the nanoparticle suspension. The resulting mixture was heated to 80 °C for 45 min to ensure complete oxidation of the iron oxide phase, to γ-Fe_2O_3. After another treatment with 10% nitric acid, the suspension was washed twice with acetone and diethyl ether and re-dispersed in the desired amount of water.

Magnetic polymer preparation. 1 mol% phenylbis (2,4,6-trimethylbenzoyl)phosphine oxide (BAPO) was dissolved in trimethylolpropane ethoxylate triacrylate (Mn 912 g mol^{-1}) by magnetically stirring the mixture overnight in the absence of light. Once the BAPO was fully dissolved in 10 mL TET solution, NF-TET suspension was prepared by addition of μL volumes of concentrated aqueous nanoflower suspension to achieve the required concentration. The mixture was then vortexed until the suspension was completely homogeneous, the nanoparticle-monomer suspension was then stored away from direct light. The NF-TET suspension was then transferred into a polydimethylsiloxane (PDMS) template containing (1 × 3 mm, h × d) cylindrical wells. The wells were exposed to the UV source for 5 minutes at which point complete polymerization was observed. The magnetic polymer cylinders were then magnetically isolated and washed several times with ethanol and with deionized water.

Adsorption measurements. A MB stock solution of fixed concentration was prepared, and the pH adjusted to the desired concentration using 0.1 M HCl or NaOH and a pH meter. 5 mL of the stock solution was added to a single use glass vial containing the desired mass of adsorbent for analysis. The vial was placed on a shaker, at room temperature for a defined period of time. The supernatant was isolated and analysed by UV-visible spectroscopy. The dye removal% and the adsorption capacity (q) were quantified by measuring adsorption at the λ_{max} (665 nm) and could be calculated using the following equations: All

measurements were undertaken at laboratory temperature which ranged from 19–22 °C.

$$\text{Dye removal}(\%) = \frac{(C_0 - C_e)}{C_0} \times 100 \quad (1)$$

$$q = \frac{(C_0 - C_e)}{m} V \quad (2)$$

where C_0 and C_e represent the initial and equilibrium dye concentrations in mg L^{-1}, m is the mass of the adsorbent used in g, and V is the volume of the dye solution in L.

Reusability. Adsorbents were transferred to a round bottom flask with cooling condenser containing 100 mL of EtOH, the solvent was heated at 50 °C for 1 h at which point no visible dye remained in the polymer. The polymer structures were then isolated and rinsed several times with DI water. The EtOH was then removed using a rotary evaporator, allowing the dissolved MB to be isolated and quantified gravimetrically.

Dynamic light scattering. DLS measurements were undertaken using a Malvern Nano ZetaSizer (Malvern Instruments, Malvern UK). The data was processed using the dispersion technology software (v 7.13, Malvern instruments, Malvern UK) with the multiple narrow modes algorithm to calculate the hydrodynamic diameter and Polydispersity Index (PDI). All measurements were performed three times, the average with standard deviation was reported.

Conflicts of interest

The authors declare that they have no known competing financial interests or personal relationships that could have appeared to influence the work reported in this paper.

Data availability

Data for this article are available on request from the corresponding author. Supplementary Information (SI) is available. See DOI: https://doi.org/10.1039/d5su00701a.

Acknowledgements

This work has been conducted with the financial support of Research Ireland (RI), formerly Science Foundation Ireland (SFI), the authors acknowledge their financial support under 16/IA/4584. C. D. acknowledges funding from Research Ireland under the Pathway Programme (Grant No. 22/PATH-S/10790). L. F. acknowledges funding from Research Ireland under the Frontiers for the Future Programme (Grant No. 22/FFP-P/11541). We would also like to acknowledge Dr Demetra Achilleos for helpful comments.

References

1 F. Mashkoor and A. Nasar, *J. Magn. Magn. Mater.*, 2020, **500**, 166408.
2 L. Chlebkova, V. Vaclavik, T. Dvorsky and R. Zajac, *IOP Conf. Ser. Earth Environ. Sci.*, 2020, **444**, 012024.
3 O. A. Shabaan, H. S. Jahin and G. G. Mohamed, *Arabian J. Chem.*, 2020, **13**, 4797–4810.
4 C. Zhu, F. Qi-ming, H. Ma, M. Wu, D. Wang and Z. Wang, *BioResources*, 2018, **13**, 6033–6046.
5 R. H. Schirmer, H. Adler, M. Pickhardt and E. Mandelkow, *Neurobiol. Aging*, 2011, **32**, 2325.e2327.
6 P. O. Oladoye, T. O. Ajiboye, E. O. Omotola and O. J. Oyewola, *Results Eng.*, 2022, **16**, 100678.
7 I. Khan, K. Saeed, I. Zekker, B. Zhang, A. H. Hendi, A. Ahmad, S. Ahmad, N. Zada, H. Ahmad, L. A. Shah, T. Shah and I. Khan, *Water*, 2022, **14**, 242.
8 Y. Wang, Y. Xie, Y. Zhang, S. Tang, C. Guo, J. Wu and R. Lau, *Chem. Eng. Res. Des.*, 2016, **114**, 258–267.
9 M. M. Hasan, M. A. Shenashen, M. N. Hasan, H. Znad, M. S. Salman and M. R. Awual, *J. Mol. Liq.*, 2021, **323**, 114587.
10 K. B. Tan, M. Vakili, B. A. Horri, P. E. Poh, A. Z. Abdullah and B. Salamatinia, *Sep. Purif. Technol.*, 2015, **150**, 229–242.
11 C. F. Mok, Y. C. Ching, F. Muhamad, N. A. Abu Osman, N. D. Hai and C. R. Che Hassan, *J. Polym. Environ.*, 2020, **28**, 775–793.
12 P. A. Alaba, N. A. Oladoja, Y. M. Sani, O. B. Ayodele, I. Y. Mohammed, S. F. Olupinla and W. M. W. Daud, *J. Environ. Chem. Eng.*, 2018, **6**, 1651–1672.
13 G. Crini, *Bioresour. Technol.*, 2006, **97**, 1061–1085.
14 G. A. Adebisi, Z. Z. Chowdhury and P. A. Alaba, *J. Cleaner Prod.*, 2017, **148**, 958–968.
15 R. Sivakumar and N. Y. Lee, *Chemosphere*, 2022, **286**, 131890.
16 S. Dutta, B. Gupta, S. K. Srivastava and A. K. Gupta, *Mater. Adv.*, 2021, **2**, 4497–4531.
17 G. Bayramoglu, B. Altintas and M. Y. Arica, *Chem. Eng. J.*, 2009, **152**, 339–346.
18 M. M. Hassan and C. M. Carr, *Chemosphere*, 2018, **209**, 201–219.
19 D. Yanardağ and S. Edebali, *Biomass Convers. Biorefin.*, 2024, **14**, 5699–5710.
20 C. Li, X. Wang, D. Meng and L. Zhou, *Int. J. Biol. Macromol.*, 2018, **107**, 1871–1878.
21 X. Qi, X. Tong, W. Pan, Q. Zeng, S. You and J. Shen, *J. Cleaner Prod.*, 2021, **315**, 128221.
22 H.-J. Zhang, J.-H. Wang, Y.-H. Zhang and T.-L. Hu, *J. Polym. Sci., Part A: Polym. Chem.*, 2017, **55**, 1329–1337.
23 N. Taheri and M. Dinari, *Appl. Surf. Sci. Adv.*, 2023, **18**, 100543.
24 L. R. Bonetto, F. Ferrarini, C. de Marco, J. S. Crespo, R. Guégan and M. Giovanela, *J. Water Proc. Eng.*, 2015, **6**, 11–20.
25 R. Sivashankar, A. B. Sathya, K. Vasantharaj and V. Sivasubramanian, *Environ. Nanotechnol. Monit. Manag.*, 2014, **1–2**, 36–49.
26 O. Moradi and G. Sharma, *Environ. Res.*, 2021, **201**, 111534.
27 Y. Zhang, X. Hong, X.-M. Cao, X.-Q. Huang, B. Hu, S.-Y. Ding and H. Lin, *ACS Appl. Mater. Interfaces*, 2021, **13**, 6359–6366.
28 Y. e. Cheng, Y. Chen, M. He, N. Zhou, X. Meng, Z. Dai and Y. Xiong, *Sep. Purif. Technol.*, 2024, **335**, 126119.
29 Y. Zhao, X. Tao, B. Xu, W. Liu and S. Lin, *Adv. Funct. Mater.*, 2024, **34**, 2401895.

30 P. M. C. Matias, D. Murtinho and A. J. M. Valente, *Polymers*, 2023, **15**.
31 A. Sanjabi, S. Azizian, M. Torabi, M. A. Zolfigol and M. Yarie, *Microporous Mesoporous Mater.*, 2023, **348**, 112367.
32 S. Chatterjee, K. Ghosal, M. Kumar, S. Mahmood and S. Thomas, *J. Drug Delivery Sci. Technol.*, 2023, **79**, 104095.
33 M. Ahmadian and M. Jaymand, *Coord. Chem. Rev.*, 2023, **486**, 215152.
34 T. S. Anirudhan and A. R. Tharun, *Chem. Eng. J.*, 2012, **181–182**, 761–769.
35 S. Emik, S. Işık and E. Yıldırım, *J. Polym. Environ.*, 2021, **29**, 1963–1977.
36 K. Wang, J. Fu, S. Wang, M. Gao, J. Zhu, Z. Wang and Q. Xu, *J. Colloid Interface Sci.*, 2018, **516**, 263–273.
37 C. Jiang, X. Wang, D. Qin, W. Da, B. Hou, C. Hao and J. Wu, *J. Hazard. Mater.*, 2019, **369**, 50–61.
38 N. You, X.-F. Wang, J.-Y. Li, H.-T. Fan, H. Shen and Q. Zhang, *J. Ind. Eng. Chem.*, 2019, **70**, 346–354.
39 R. Nithya, A. Thirunavukkarasu, A. B. Sathya and R. Sivashankar, *Environ. Chem. Lett.*, 2021, **19**, 1275–1294.
40 F. S. A. Khan, N. M. Mubarak, Y. H. Tan, R. R. Karri, M. Khalid, R. Walvekar, E. C. Abdullah, S. A. Mazari and S. Nizamuddin, *Environ. Sci. Pollut. Res.*, 2020, **27**, 43526–43541.
41 F. Ge, H. Ye, M.-M. Li and B.-X. Zhao, *Chem. Eng. J.*, 2012, **198–199**, 11–17.
42 A. Afkhami, M. Saber-Tehrani and H. Bagheri, *Desalination*, 2010, **263**, 240–248.
43 W. Wang, Z. Ding, M. Cai, H. Jian, Z. Zeng, F. Li and J. P. Liu, *Appl. Surf. Sci.*, 2015, **346**, 348–353.
44 R. Singh, V. Munya, V. N. Are, D. Nayak and S. Chattopadhyay, *ACS Omega*, 2021, **6**, 23139–23154.
45 T. J. Mooibroek, P. Gamez and J. Reedijk, *CrystEngComm*, 2008, **10**, 1501–1515.
46 E. P. McKiernan, C. Moloney, T. Roy Chaudhuri, S. Clerkin, K. Behan, R. M. Straubinger, J. Crean and D. F. Brougham, *Acta Biomater.*, 2022, **152**, 393–405.
47 S. Yang, F. Shiyu, Z. Yiming, X. Chuanlong and X. and Li, *Int. J. Polym. Mater. Polym. Biomater.*, 2010, **60**, 62–74.
48 J. Rogowska, M. Cieszynska-Semenowicz, W. Ratajczyk and L. Wolska, *Ambio*, 2020, **49**, 487–503.
49 I. Pavlakos, T. Arif, A. E. Aliev, W. B. Motherwell, G. J. Tizzard and S. J. Coles, *Angew. Chem., Int. Ed.*, 2015, **54**, 8169–8174.
50 K. Fang, K. Li, T. Yang, J. Li and W. He, *Int. J. Biol. Macromol.*, 2021, **184**, 509–521.
51 B. Zeng, L. Yang, W. Zheng, J. Zhu, X. Ma, X. Liu, C. Yuan, Y. Xu and L. Dai, *J. Mater. Sci. Technol.*, 2018, **34**, 999–1007.
52 T. Tatarchuk, L. Soltys and W. Macyk, *J. Mol. Liq.*, **223**(384), 122174.
53 S. Lyons, E. P. McKiernan, D. F. Brougham and A. Morrin, *Nanoscale*, 2020, **12**, 10550–10558.
54 P. Hugounenq, M. Levy, D. Alloyeau, L. Lartigue, E. Dubois, V. Cabuil, C. Ricolleau, S. Roux, C. Wilhelm, F. Gazeau and R. Bazzi, *J. Phys. Chem. C*, 2012, **116**, 15702–15712.